INFOCUS

LIGIM Internal Report

October 1996

Introduction

It is necessary to create geometrical models of the patient's body shape (external) and the treatment volumes (internal) and to correlate these two models in the same reference system.

As a first step we will neglect the movements of the patient and assume that the shapes involved are unchanged during the treatment. The objective is to develop tools to improve the initial positioning of the patient and to enable dosimetric calculations to proceed on a much more realistic geometry than is currently the case. Three tasks will need to be performed to realise this objective.

- development of the external model
- development of the internal model
- correlation between the two models

For the dynamic models: first we can consider movement of the parts as rigid bodies and secondly we can tackle the most general case of movement as deformable bodies.

1 Reconstruction with surface model

1.1 Internal static model

Our goal is the reconstruction of a smooth closed surface from planar contours of a volume.

The contours are defined to be very simple: they are parallel slices with one single contour by slice, so there are no objects with branchs (Fig. 1). That way we avoid numerous problems of matching between slices [EPO91, Mey94].

1.1.1 Uniform B-spline surfaces

Each contour contains the same number of points. A uniform *B-spline* surface is then constructed to fit these points :

$$P(u,v) = \sum_{i=0}^{n} \sum_{j=0}^{m} P_{ij} N_i^k(u) N_j^l(v) \tag{1}$$

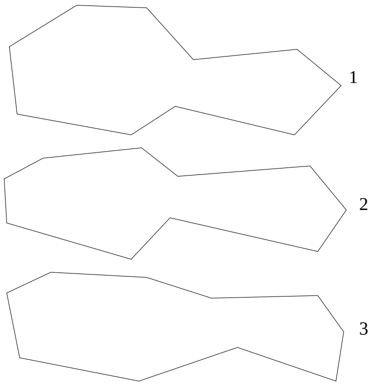

Figure 1: Example of contours

where :

$0 \leq u \leq 1$ and $0 \leq v \leq 1$

$m+1$	: number of contours
$n+1$	: number of points on each contour
k, l	: degree in the u and v directions
P_{ij}	: control points
$N_i^k(u)$ et $N_j^l(v)$	: spline basis

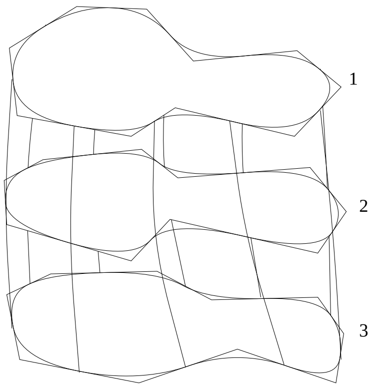

Figure 2: Contours interpolated by a spline surface

Equation (1) describes a biderectional curve scheme. The basis functions are bivariate functions of u and v which are constructed as products of univariate basis functions. As the curves on each contour represent closed curves, the isoparamtric curves in the u direction should also represent closed curves.

Therefore we can take the last point equal to the first one to obtain a closed *B-spline* curve but this introduced a discontinuity at this point, as shown on figure (3).

1.1.2 Periodic uniform B-spline surfaces

We use periodic uniform *B-spline* curves in the u direction to solve the discontinuity problem. The periodic uniform curves are defined from open *B-spline* curves:

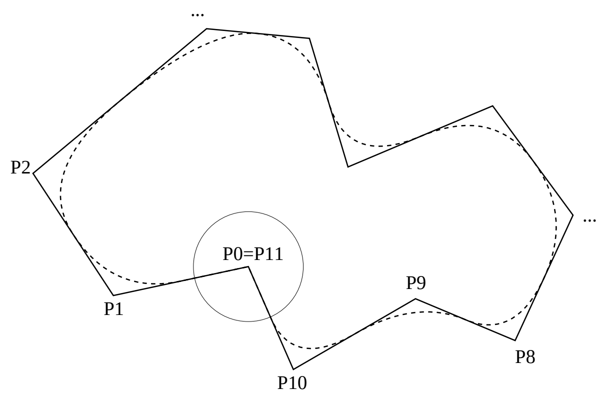

Figure 3: Discontinuity for $u = 0$ and $u = 1$

$$P(u) = \sum_{i=0}^{n} P_i N_i^k(u) \text{ for } u \in [0;1] \tag{2}$$

with p_i for $i = 0 \dots n$, control points and k the degree of the spline.
and $\{u_j\}$ a uniform knot sequence :

$$\underbrace{0,\ \dots,\ 0}_{k+1 \text{ times}},\ \frac{1}{n},\ \frac{2}{n},\ \dots\dots,\ \frac{n-1}{n},\ \underbrace{1,\ \dots,\ 1}_{k+1 \text{ times}}$$

To obtain a periodic curve and ensure that the C^{k-1} continuity is respected at point $P(0) = P(1)$, $(k-1)$ points are added:

$$P_{n+i} = P_{i-1} \text{ with } i = 1, \dots, k-1$$

and a new knot sequence $\{u_j\}$ is defined

$$-\frac{k-1}{n},\ \dots,\ -\frac{1}{n},\ 0,\ \dots\dots,\ 1,\ \frac{n+1}{n},\ \dots,\ \frac{n+k-1}{n}$$

So we define a *B-spline* curve:

$$P(u) = \sum_{i=0}^{n+k+1} P_i N_i^k(u) \text{ on } u \in [0;1]$$

which corresponds to a periodic *B-spline*

$$P(u) = \sum_{i=0}^{n} P_{i\,mod(n+1)} N_{i\,mod(n+1)}^k \text{ with } u \in \mathbb{R}$$

defined and C^{k-1} continuous on $\mathbb{R}$.

1.2 Results

The initial data are 69 planar outlines of a prostate with 52 points on each contour (Fig. 4). We reconstruct this object with periodic splines surfaces of degree 3 and 15×15 control points. The reconstruct prostate is displayed (Fig. 5) with 50×20, which corresponds to 27% of the initial data.

The initial data of the second example are 91 slices with 73 points representing a bladder (Fig. 6). We have reconstructed this object at two different resolutions of this objet: (Fig. 7 with a reduction to 2% of the initial data, and (8) and 15% of the initial data.

However we notice that the reconstructed object should be closed at its top and bottom. That will be an interesting extension of the model.

The figure (9) shows the good quality of the reconstruction since the reconstructed model fits well the initial data of a body (the data are dark,the reconstruct body are light).

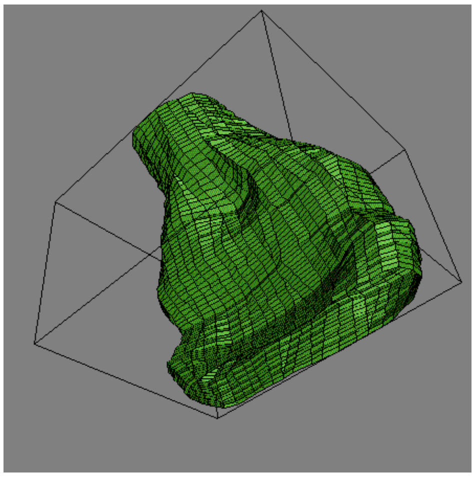

Figure 4: prostate data: 69×52 initial points

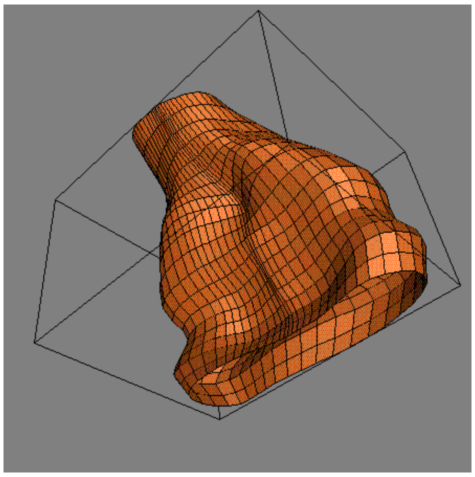

Figure 5: Prostate model : 50×20 reconstruct points

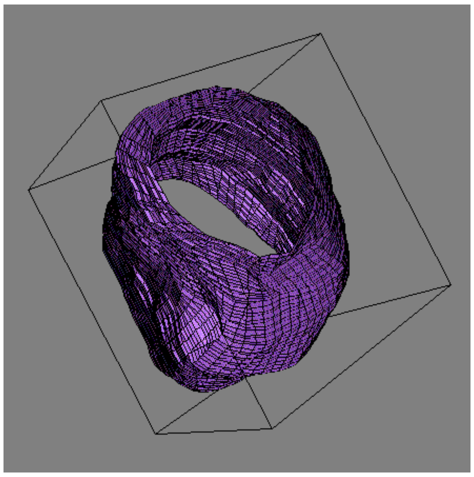

Figure 6: Bladder data : 91×73 initial points

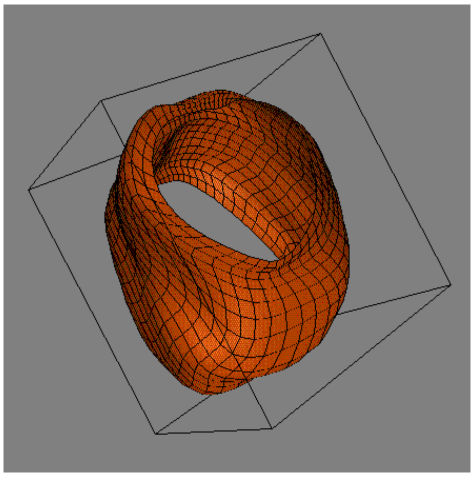

Figure 7: Bladder model : 15×10 reconstruct points

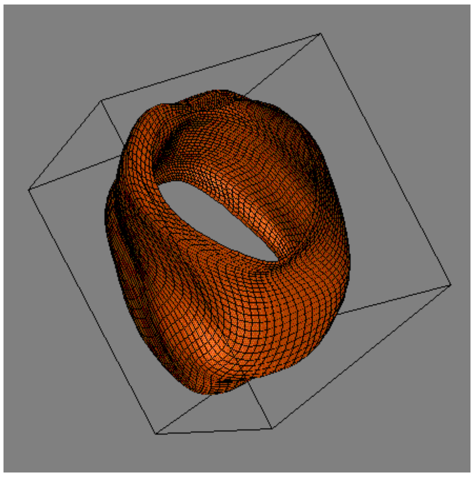

Figure 8: Bladder model : 50×20 points

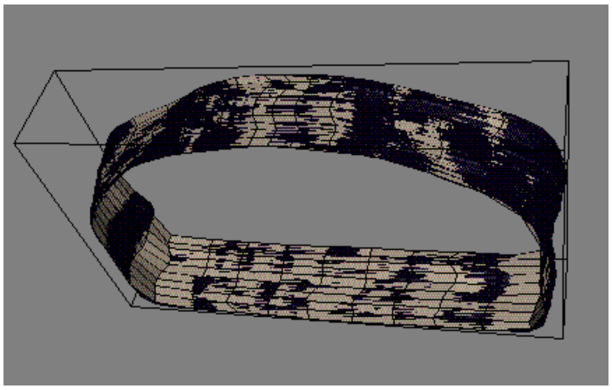

Figure 9: Body : 79×127 initial points and 50×20 reconstruct points

2 Multiview Range Data Registration

2.1 Introduction

The definition of two digitized forms (two clouds of points) in the same reference system necessitates the calculation of a rigid transformation allowing to map one of the clouds into the reference frame of the other cloud. Unfortunately, due to the measurement error as well as the deformation of the measured object it is unlikely that any rigid transformation exactly maps the cloud.

To solve this problem we have developped an iterative method that registates images of the same objet (the patient) from different views and at different times. We use an optimisation method. For this we estimate an initial transformation wich will be refined.

2.2 Initial matrix

We have two range images taken from two points of view of the same object. The difficulty is to find an good initial transformation to ensure that the iterative process converges.

To initialise the registration, we need a rigid transformation between the two images. For this we calculate the homogeneous transformation matrix between four points $\{P_i\}_{i=0,\ldots,3}$ from the first cloud and the same four points $\{P'_i\}_{i=0,\ldots,3}$ from the second (Fig. 10). In fact these points are feature points that have been detected on both images. The rigid transformation $\mathcal{T}_r$ can be defined by:

$$\mathcal{T}_r(P_i) = R.P_i + d = P'_i$$

where :
- R Rotational matrix
- d translation

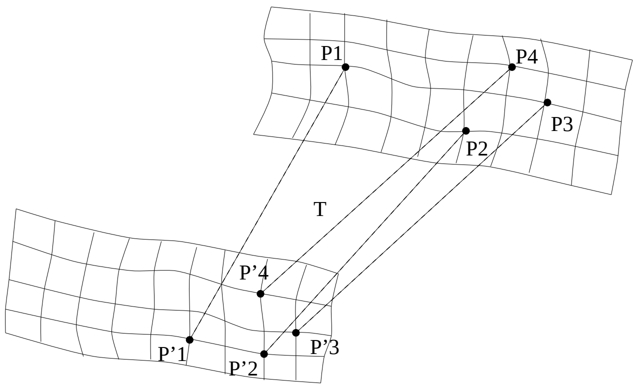

Figure 10: Initial transformation determination

For the moment we determine the initial points manually. Some circular markers are placed on the object and the gravity center of the digitezed image of each marker gives a feature point.

However, some problems may rise due to the use of markers:

- markers need to remain on the patient's body during the treatment
- three non aligned points are sufficient, but they should be present on each image
- the localisation of the gravity center is no so easy, some errors are introduced

For all these reasons, it is necessary to use anatomical references for the registration: crest lines, edges, singular points ...

2.3 Iterative registration

Next we apply an iterative process from the initial matrix $\mathcal{T}_I$.

We extract points from the first cloud by uniform sampling (for example 1 out of 10 horizontally and vertically). Then these points are mapped to the points of the second cloud by a rigid transformation. This is a point to point registration.

We affect a cost to this mapping, wich depends on the euclidian distance. So we have :

$$cost(\mathcal{T}) = \frac{\sum_{P_i \in Sampling} \left[dist(\mathcal{T}(P_i) - Q_i)\right]^2}{N}$$

where :

$\mathcal{T}(P_i)$	is the image of P_i after the transformation $\mathcal{T}$
Q_i	is the nearest point of $\mathcal{T}(P_i)$ in the second cloud
N	is the number of sampled points

and $dist(\mathcal{T}(P_i) - Q_i) = \begin{cases} \text{euclidian distance} & \text{if } d \leq treshold \\ 0 & \text{si } d > treshold \end{cases}$

Figure (11) illustrates this process in 2D.

Therefore the points that are not close enough are not taken into consideration. In practice, the treshold is taken as twice the distance between points from the second cloud.

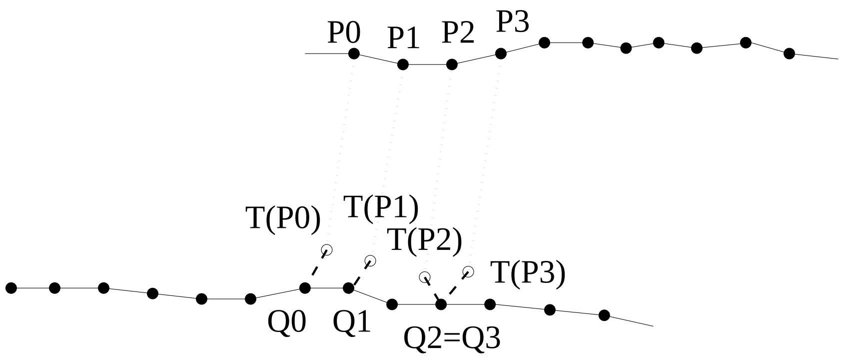

Figure 11: Cost calculation

However, if the clouds are far from each other, the ditance is greather than the treshold and the cost will be zeroed. So we define a modified cost :

$$cost(\mathcal{T}) = \frac{\sum_{P_i \in Sampling} [dist(\mathcal{T}(P_i) - Q_i)]^2}{N'}$$

with N' the number of points wich have an associated point in the other cloud for this transformation.

The aim is to find a transformation $\mathcal{T}$ which minimizes this cost. We calculate the new necessary twelve parameters of the homogeneous matrix by a linear method.

We repeat this while the cost is greather than a specified treshold

The following algorithm illustrates the registration method :

- Determination of feature points P_{1i} and P_{2i} for $i = 0, \ldots, 3$
- Calculation of $\mathcal{T}_0$
- $\mathcal{T} = \mathcal{T}_0$
- do
  - For each point P_i sampled in cloud #1
    - Compute $\mathcal{T}(P_j)$
    - Compute Q_j so that for $(Q_j \in cloud\#2)$, $d_j = dist(\mathcal{T}(P_j) - Q_j)$ is minimal
    - if $d_j \geq seuil$
      - then $d_j = 0$
      - else $N' \leftarrow N' + 1$
  - Calculate $\mathcal{T}'$ by linear method
  - $\mathcal{T} = \mathcal{T}'$
- while $(cost(\mathcal{T}) > value)$

So we have defined the mathematical tools to express two range images in the same reference system.

2.4 Results

Figures (12) and (13) show the results of the registration of two clouds of 12000 points each, representing a pipe. The two images overlap nearly totally.

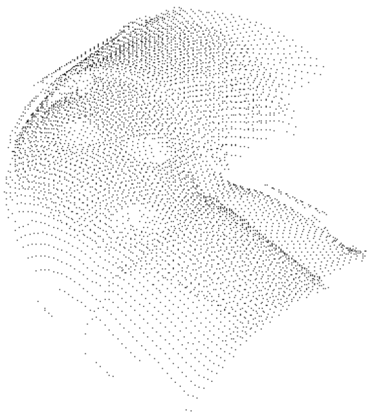

Figure 12: Initial data

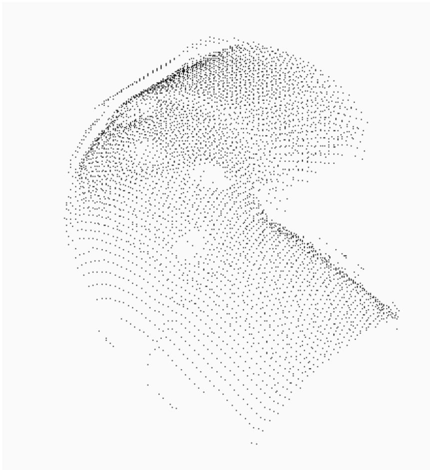

Figure 13: After 50 iterations

Figures (14) et (15) show the registration between two images of different parts of a foot, with partial overlapping.

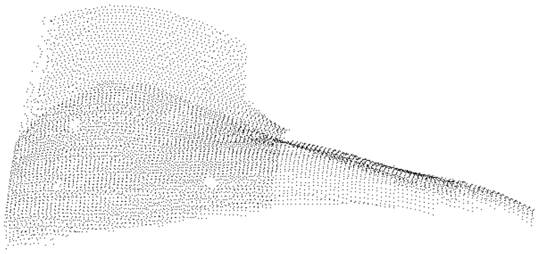

Figure 14: Initial data

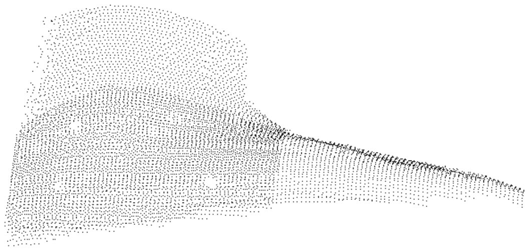

Figure 15: After 50 iterations

We notice that the registration is quite long and that the precision depends greatly on marker's position.

So we will tend to iterative registration method but without markers :

- by projection 3D/2D [FAB94];
- by motion in a potential field [MFVR95];
- by registration of lines or singular points extracted from anatomical references [DSTA95, SC94].

3 Reconstruction with particle system

3.1 Particle systems

The reconstruction of dynamical internal and external models with parametric surface models (B-spline for example) is quite difficult. Indeed, the calculation of the deformation response due to external forces on such models is not feasible.

So we tend towards a particle based model composed of ponctual masses in interaction. This model is a good compromise between display time, realism and memory occupation.

Morover, the collisions and the reaction forces are easy to handle, because particles are driven by newtonian laws of physics [Wit92] :

- unary forces (gravity) which acts independently on each particle
- n-ary forces (springs) which are applied to a finite set of particles
- forces of spatial interaction (attraction/ repulsion) which depends on the distance between two particles

3.1.1 Interaction betwwen particles

We use the classical *Lennard-Jones* potential law:

$$E(r) = \frac{\varepsilon}{m-n}\left[m\left(\frac{r_0}{r}\right)^n - n\left(\frac{r_0}{r}\right)^m\right] \tag{3}$$

where :

r_0	: stability distance
r	: distance between particles
ε	: amplitude
n et m	: define the shape of the curve (often n=2*m)

Therefore the force exerted by particle #1 on particle #2 is (Fig. 16):

$$\vec{f}_{1\to 2}(r) = \overrightarrow{grad}\,(E(r)) \text{ and } \vec{f}_{2\to 1}(r) = -\vec{f}_{1\to 2}(r) \tag{4}$$

But this force introduces oscillation around the stability position. So Lombardo, in [Lom96], proposes a new force to avoid oscillations (Fig. 16):

$$\vec{f}_{Lombardo}(r) = -\varepsilon\frac{(r_0-r)^3}{r}e^{-\alpha(r_0-r)^2}\frac{\vec{r}}{r} \tag{5}$$

where :

α : determinates the influence field of the force

We see on figures (17) and (18) that there is some overlapping particules with the Lombardo force, since there is no more a stability position but a stability zone due to the horizontal tangent at r_0.

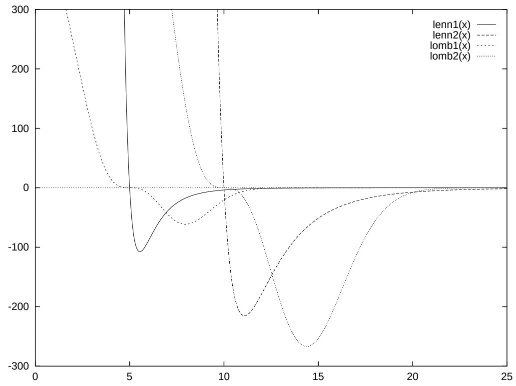

Figure 16: Interaction forces

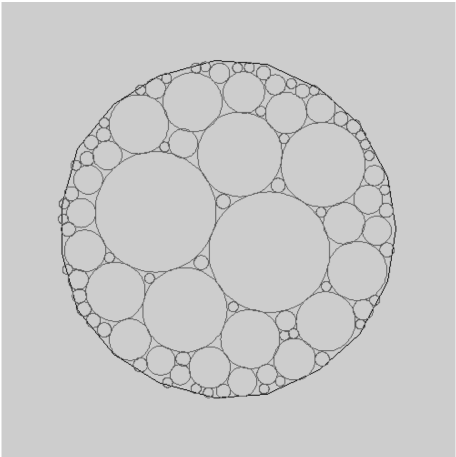

Figure 17: Lennard-Jones

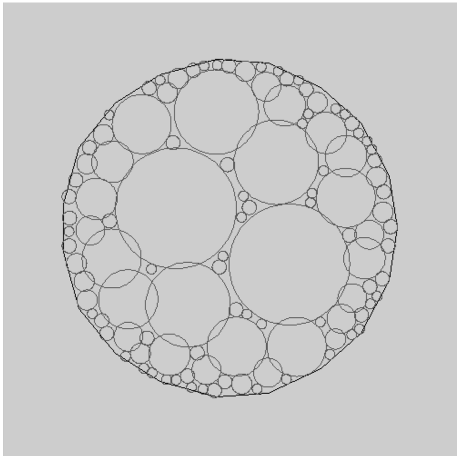

Figure 18: Lombardo

3.1.2 Collision Force

The detection problem is reduced to a problem of distance between a sphere (the particle) and a plane (the contour).

Figure (19) defines the collision response $\vec{v} = \vec{v}_t - r.\vec{v}_n$ with r the restitution coefficient.

If a particle is colliding the contour with tangential velocity equal to zero ,then there is contact (Fig. 20) and the force applied is $\vec{f_c} = -\left(\vec{n}.\vec{f}\right)\vec{f}$, so the particle slips along the contour.

3.2 Internal static model

The aim is to reconstruct a volume from 3D contours. We propose a model able to reconstruct a large variety of shapes (with branches, holes).

The process of the reconstruction with particules can be divided in several parts:

1. particles initialisation

2. repeat until the desired precision is obtained :

    - new particles generation

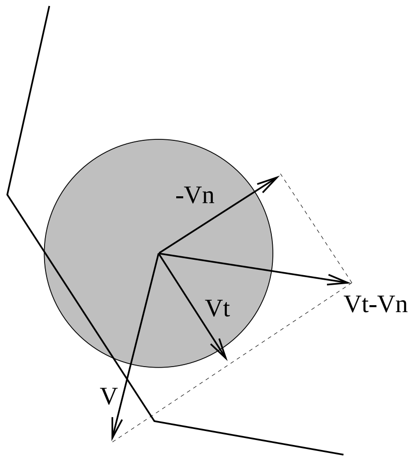

Figure 19: Collision response

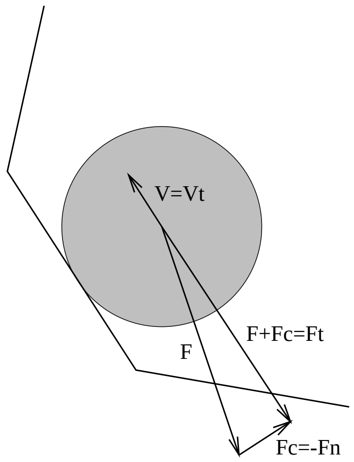

Figure 20: Contact response

- interaction and collision forces calculation
- positions calculation by integrating forces

3.2.1 Particles in layers

We use a particle system as discribed previously. Each particule is defined by:

- a position P ;
- a velocity $\vec{v}$;
- external forces $\vec{f}$;
- a radius R ;
- a masse m, proportionnal to the volume ;
- and a repulsion field r.

The repulsion field parameter is introduced to model particles in layers (Fig. 21) like in [Jim93]: nucleus, derm for deformability and skin for cohesion.

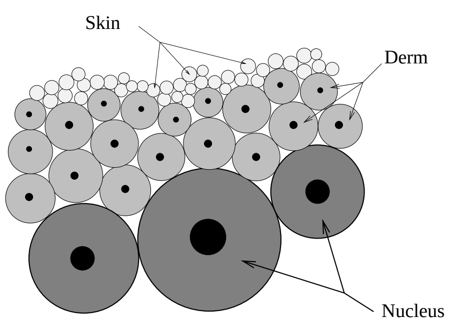

Figure 21: layers structuration

This model permits to greatly reduce the number of particles. This is illustated on figures (22) and (23). The nucleus is modeled first and then the radius of the particle is reduced and the shape of the object is refined.

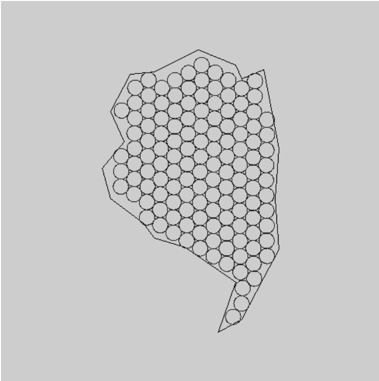

Figure 22: Monolayer : 134 particles

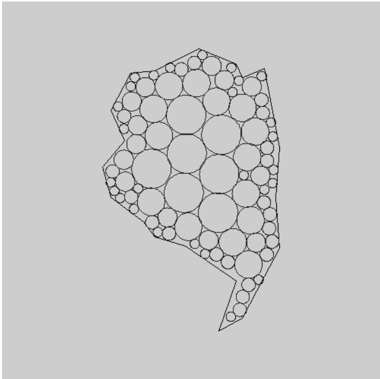

Figure 23: Multilayer : 82 particles

3.2.2 Particle generation

We define simple rules for new particle generation.

1. a new particle should not perturb the system
2. particles should be created near the equilibium position
3. particules should not be on the contour.

When it is no more possible to create a new particle, the radius and the repulsion field are decreased. We show the evolution on figure (24).

The figure (25)show the same evolution but in 3D .

Nevertheless this is not sufficient, and we should allow the particle radius to increase. On the figure (26) the reconstruction is initalized in the left cavity and propagates to the right one with only decreasing radius, while on the figure (27) an adaptative radius is employed. The number of particles is divided by two with the adaptative method.

3.3 Internal dynamic model

3.3.1 With springs

After the static object has been reconstructed with particles, we consider it not too deformable, that means that there is no important variation in its topology. A consequence is that we have a neighbourhood relation between particles which are close. This relation can be modeled with a spring (Fig.28) and this reduces the complexity.

The force exerted on particule #2 by #1 is:

$$\begin{aligned} \vec{f}_{1\to 2} &= -\left[k_s(r-l) + k_d \frac{\vec{v}.\vec{r}}{r}\right]\frac{\vec{r}}{r} \\ \text{et } \vec{f}_{2\to 1} &= -\vec{f}_{1\to 2} \end{aligned} \tag{6}$$

where :

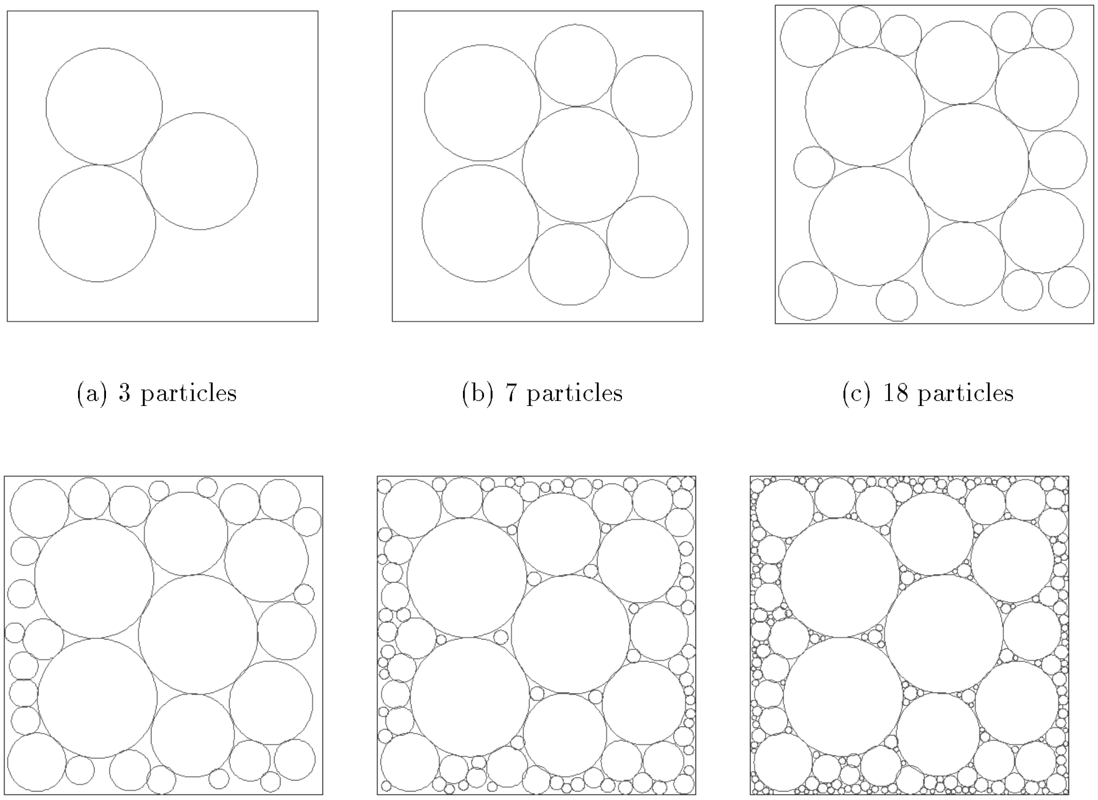

(a) 3 particles (b) 7 particles (c) 18 particles

(d) 32 particles (e) ≈100 particles (f) ≈220 particles

Figure 24: Evolution of the reconstruction of a square

k_s : spring constant
k_d : damping constant
$r = \overrightarrow{P_1 P_2}$
$v = \overrightarrow{V_1 V_2}$

The constants define the characteristics of the material: rigidity depens on the spring constant and the deformability on the damping constant. This two parameters allow to model different materials like superball or clay.

But the springs tends to increase the resistance of the object, impotant deformation are not allowed. To solve this problem the spring can be removed when the elongation is greater than a cohesion treshold and then the object can break into parts.

3.3.2 With Lennard-Jones force

We may also use the Lennard-Jones force to model the internal interactions of the object, since this force is divided in two parts : a short range repulsion and a long range attraction.

The Lennard-Jones force is used when there are constaints on deformations. For example the repulsion force prevents the particles to overlap, they slip on each other,

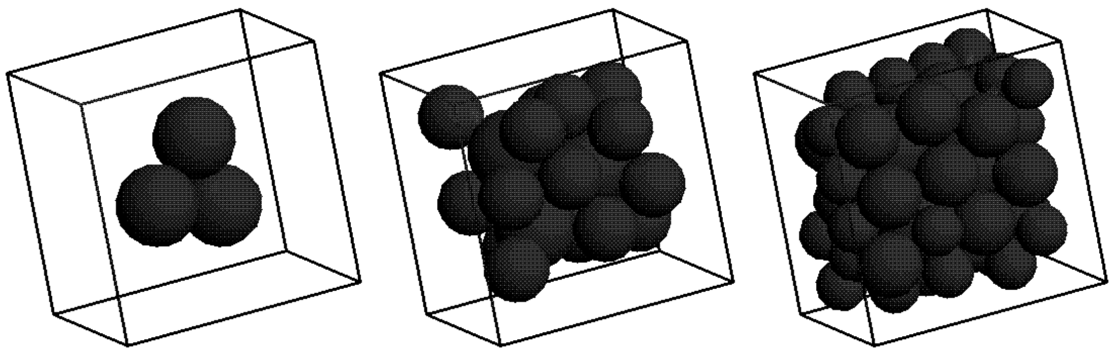

(a) 3 particles (b) 20 particles (c) 46 particles

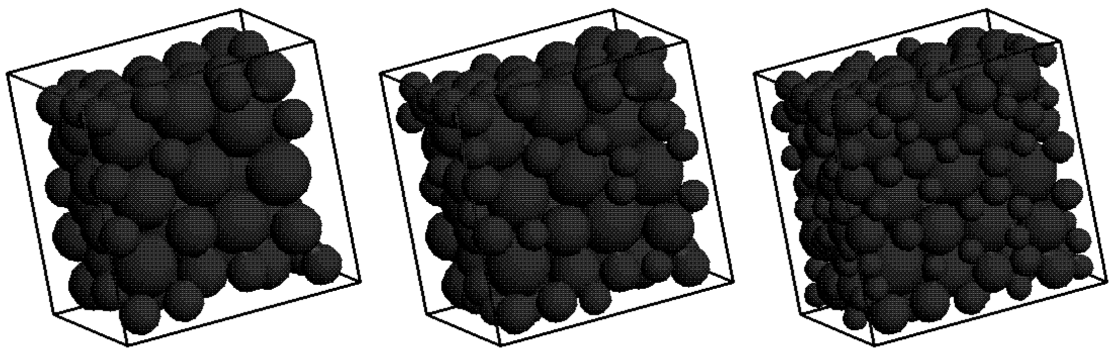

(d) 77 particles (e) 116 particles (f) 204 particles

Figure 25: Evolution of the reconstruction of a cube

and that models deformation at constant volume.

Other constraints can be defined like elasticity, malleability [PB88]. In our application, the characteristics of the organs should be defined in cooperation with physicians

3.4 External dynamic model

B-spline surfaces may be used to model the external shape, but as the precision is not so good, we prefer to use oriented particle [ST91].

The model becomes homogeneous and very simple: it comprises only particle driven by n-ary forces or forces of spatial interaction. (Fig.29).

Then very different objects can be modeled with a single particle system. For example, in our medical application:

- the external shape (the patient's body) can be represented by oriented surface particles
- the organe itself is modeled with a particle system described at section (3.2).

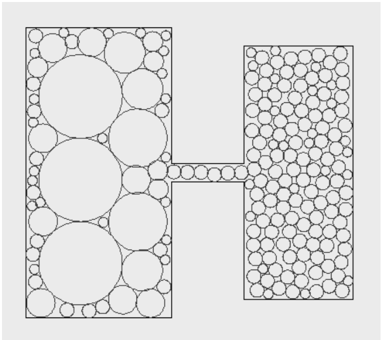

Figure 26: With decreasing radius

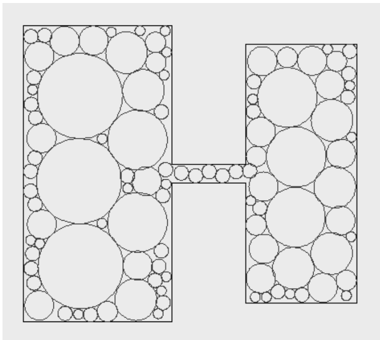

Figure 27: With adaptative radius

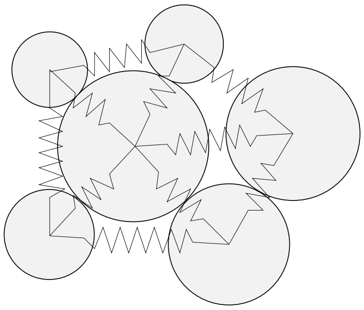

Figure 28: Springs

- the space around the organ can be modeled with particles and spatial interaction forces. Its density determinates the density of the environment

So by using particle systems we avoid the difficult problem of the calculation of collision forces and contact surfaces between objects defined by finite elements or implicit functions [DG96].

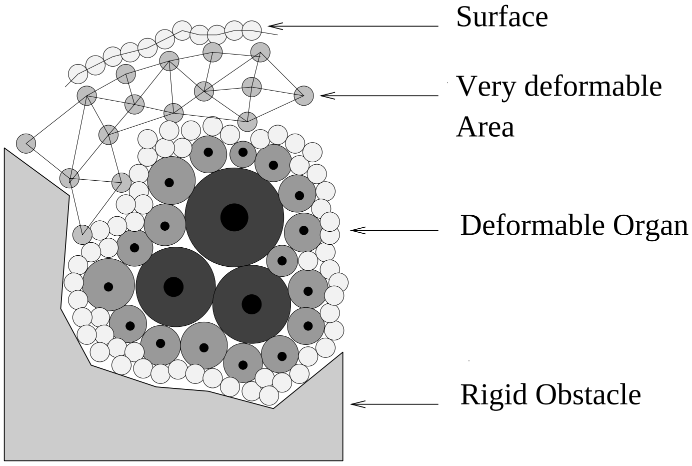

Figure 29: Complete model

References

[DG96] M. Desbrun and M.-P. Gascuel. Animation d'objets déformables à l'aide de surfaces implicites. In *4ème séminaire du groupe de travail "Animation et Simulation"*. GDR-PRC AMI (Algorithme, Modélisation et Infographie), Strasbourg, Jan. 1996.

[DSTA95] J. Declerck, G. Subsol, J-P. Thirion, and N. Ayache. Automatic retrieval of anatomical structures in 3D medical images. Technical Report 2485, INRIA, Feb. 1995. Programme 4: robotique, image et vision.

[EPO91] A. B. Ekoule, F. C. Peyrin, and C. L. Odet. A triangulation algorithm from arbitrary shaped multiple planar contours. *ACM Transactions on Graphics*, 10(2):182–199, April 1991.

[FAB94] J. Feldmar, N. Ayache, and F. Betting. 3D-2D projective registration of free-form curves and surfaces. Technical Report 2434, INRIA, Dec. 1994. Programme 4: robotique, image et vision.

[Jim93] S. Jimenez. *Modélisation et simulation physique d'objets volumiques déformables complexes.* PhD thesis, Institut National Polytechnique de Grenoble, Nov. 1993.

[Lom96] J.-C. Lombardo. *Modélisation d'objets déformables avec un système de particules orientées.* PhD thesis, Université de Grenoble I, Jan. 1996.

[Mey94] D. Meyers. *Reconstruction of surfaces from planar contours.* PhD thesis, University of Washington, 1994.

[MFVR95] G. Malandain, S. Fernandez-Vidal, and J.M. Rocchisani. Physically based rigid registration of 3D free-form objects: application to medical imaging. Technical Report 2453, INRIA, Jan. 1995. Programme 4: robotique, image et vision.

[PB88] J. C. Platt and A. H. Barr. Constraint method for flexible models. In *Proceedings of SIGGRAPH'88*, pages 279–288. Computer Graphics, 1988.

[SC94] R. Szeliski and J. Coughlan. Spline-based registration. Technical Report CRL 94-1, DEC, Cambridge Research Lab, April 1994.

[ST91] R. Szeliski and D. Tonnesen. Surface modeling with oriented particle systems. Technical Report CRL 91/14, DEC, Cambridge Research Lab, Dec. 1991.

[Wit92] A. Witkin. Particle system dynamics. In *ACM SIGGRAPH'92 Courses Notes: An introduction to physically based modeling*, pages C1–C12, july 1992.

Contents